Four point probe structures with buried and surface electrodes for the electrical characterization of ultrathin conducting films

A.W. Groenland[1], R.A.M. Wolters[1,2], A.Y. Kovalgin[1] & J. Schmitz[1]

[1] MESA+ Institute for Nanotechnology, Chair of Semiconductor Components

University of Twente, P.O. Box 217, 7500 AE Enschede, The Netherlands.

Tel +31 (0)53 489 2645, Fax +31 (0)53 489 1034

Email: A.W.Groenland@utwente.nl

[2] NXP-TSMC Research Center, High Tech Campus 4, 5656 AA Eindhoven, The Netherlands

ABSTRACT

Test structures for the electrical characterization of ultrathin conductive films are presented based on electrodes on which the ultrathin film is deposited. Two different designs are discussed: a novel design with buried electrodes and a conventional design with electrodes at the surface. This work includes test structure design and fabrication, and the electrical characterization of ALD TiN films down to 4 nm. We demonstrate that the novel test structures provide the same results as the conventional structures, and have the advantage of broader materials choice (i.e. conductor-dielectric combination). The proposed structures can be used successfully to characterize sub 10 nm films.

INTRODUCTION

Conducting thin films (sub 10 nm) have interesting applications e.g. in the field of diffusion barriers for copper metallization and phase change memories [1-4]. Electrical properties can be measured using the four probe method [5, 6]. For these thin films, van der Pauw structures (vdPs) and Greek Crosses (GCs) are commonly used [7]. However, making electrical contacts to these thin films, using planar technology, is extremely difficult; e.g. etching a via in the SiO_2 layer for the contact to such a film requires a very high selectivity. In practice, this is only possible for some SiO_2-metal combinations [8]. Enderling and co-workers proposed to use suspended Greek Crosses to overcome this problem. However, this is only suitable for films with a poor step coverage (e.g. deposited via physical vapour deposition (PVD))[9]. Giraudet and co-workers used test structures with predefined metal electrodes for the electrical characterization of thin films with good step coverage such as spin-coated conducting polymers [10].

In this work special test structures are presented to measure the electrical properties of ultrathin films in a controlled way without the need of a highly selective SiO_2–to-metal etch. These test structures (‘design A’) can be used for thin films in general, i.e. independent of film step coverage. In ‘design A’, electrodes are fabricated, which are buried in a planarized dielectric film. A thin film is deposited on top of the electrodes by means of atomic layer deposition (ALD). The thin film is characterized using the predefined electrode structures, such as the aforementioned vdPs and GCs.

Subsequently, a second set of conventional test structures (‘design B’) is fabricated to verify the results obtained from ‘design A’. In ‘design B’, the thin film is deposited directly on top of predefined electrodes without planarization. Due to the (nearly) perfect step coverage of the ALD process, this results in a good electrical contact to the ALD thin film.

‘Design A’ results in test structures (vdP & GC) with small (‘point-like’) contacts to the flat ALD thin film, while ‘design B’ yields (only) GC structures with large contact area’s to the ALD thin film following the electrode topography. Test structures in ‘design B’ are easier to manufacture, they require less process steps and no (difficult) planarization as in ‘design A’. However, they cannot be used for very thin films having a poor step coverage such as e.g. sputtered or evaporated films. Contrary, the structures of ‘design A’, are not limited by step coverage. ALD is chosen as deposition method in ‘design A’ in order to be able to compare the results directly with test structures of ‘design B’.

TEST STRUCTURE DESIGN, LAYOUT AND FABRICATION

A. ‘Design A’

Square structures are etched in a layer of 0.5 µm thermally grown SiO_2 on top of a standard silicon wafer using wet chemical etching (Fig. 1a) in buffered HF (BHF). After an additional oxidation step to insulate the silicon substrate, a layer of 70 nm TiW is sputtered and patterned using wet chemical etching in a hydrogen peroxide (H_2O_2) and ammonia (NH_4OH) to make the electrodes and connections (Fig. 1b). Subsequently a layer of 1 µm PECVD SiO_2 is deposited (Fig. 1b) and the structure is planarized using chemical mechanical polishing (CMP) (Fig. 1c). On this surface the thin ALD TiN film is deposited from titanium tetrachloride ($TiCl_4$) and ammonia (NH_4OH) at 425 °C. The ALD TiN layer is passivated by *in situ* ALD Al_2O_3 (16 nm) and *ex situ* PECVD SiO_2 layers (50 nm) (Fig. 1d). After patterning the ALD TiN and passivation layers (Fig. 1e) in H_2O_2 + NH_4OH and BHF, an additional 50 nm PECVD SiO_2 passivation layer is deposited. Next, vias are etched in BHF towards the buried electrode connections and filled with aluminium to realize contact pads (Fig. 1f). Patterning the aluminum finalizes the structures.

Using this process architecture, a variety of vdP and GC structures have been realized. A set of vdP structures was designed with different probe-to-probe spacings (*A*) and with different contact-to-edge-distances (*y*) according to fig 2a. This was done to account for alignment errors and process variations. Furthermore, a set of GC structures was designed with different *W* values, according to fig 2b. The Greek Cross is designed with the arm length *L* equal to 2.5 times the width *W*. This reduces the error in the extracted sheet resistance to < 1% while maintaining maximum sensitivity and minimal Joule heating in the arms of the cross[11-13]. VdP and GC structures were placed in a die (see Fig 3) which was replicated 81 times over a 100 mm wafer. An example of a realized van der Pauw structure is shown in Fig. 4. Using these test structures, 4 and 7 nm ALD TiN layers were electrically characterized.

B. 'Design B'

A layer of 100 nm TiN is deposited via reactive sputtering of on top of a planar multilayer structure (standard silicon wafer passivated by a layer of 100 nm LPCVD low stress silicon rich nitride (SiRN) and 100 nm PECVD SiO_2). Next, the wafer is annealed by a rapid thermal anneal (RTA) for 30 s at 450 °C in nitrogen (N_2). The TiN layer is patterned using wet chemical etching in a mixture of hydrogen peroxide (H_2O_2) and ammonia (NH_4OH) to make the electrodes (Fig. 5a). Subsequently, the thin ALD TiN film is deposited which is passivated by *in situ* ALD Al_2O_3 (16 nm) and *ex situ* PECVD SiO_2 (50 nm) layers. After patterning the ALD TiN and passivation layers in H_2O_2 + NH_4OH and BHF (Fig. 5b), an additional 50 nm PECVD SiO_2 passivation layer is deposited. Next, vias are etched in the ALD TiN passivation in BHF and filled in with sputtered aluminium to become contact pads (Fig. 5c). This via etch can be carried out without the need for a highly selective SiO_2–to-metal etch; the etch is terminated in the (thick) underlying TiN electrode without losing electrical contact to the ALD TiN thin film. Patterning the aluminum finalizes the structures.

In this process architecture, only GC devices with a similar design as in 'design A' (see fig 4b) with *W*-values of 8 and 50 μm are realized; vdP-type structures are not trivial to be technologically implemented within this process architecture. Both 8 and 50 μm GC devices are part of a test die, which is replicated 44 times over a 100 mm wafer. An example of a realized Greek Cross structure is shown in Fig. 6.

EXPERIMENTAL

The layer thickness of the ALD TiN films is determined using a Woollam M2000 Spectroscopic Ellipsometer (SE) in the energy range 0.7-5 eV. Measurements were taken *in situ* directly after deposition. From the recorded SE data, the ALD TiN layer thickness is derived using a model containing the optical constants of all sub-layers, which is calibrated against HRSEM measurements [14]. The contact area of the electrodes is verified by HRSEM on cross-sections of the sample (Fig 7).

For the electrical characterization, *IV*-measurements were carried out using a HP4156B or Keithley 4200 precision semiconductor parameter analyser in combination with a Cascade Microtech probe station. For the measurements at elevated temperatures, the temperature controlled chuck of the probe station was used.

RESULTS

A. Measurements at room temperature ('Design A')

For a 7 nm ALD TiN layer, *IV*-curves are measured from van der Pauw and Greek Cross structures having probe-to-probe distances *A* (vdP) or *W* values (GC) in the range of 10 to 300 μm. All devices are measured over all 4 orientations. The *IV*-curves for one of the four orientations are shown for vdPs (Fig. 8a) and GCs (Fig. 8b). For both sets of devices, linear *IV*-behaviour is observed. This is confirmed by plotting $d(V_m)/d(I_m)$, which is a constant function of I_m (see insets in Fig. 8).

From (solely) the slope of both sets of *IV*-curves, the ('measured') resistance ($R_m = V_m/I_m$) is calculated and averaged over the 4 orientations. The results are shown in Fig. 9a. In Fig. 9b R_m values are shown for a 4 nm ALD TiN layer. Values of R_m extracted from a van der Pauw device with a probe-to-probe distance of 300 μm are included in the graphs.

For van der Pauw structures, a relatively large spread in the *IV*-characteristics (Fig. 8a) is observed for different device dimensions and also between different orientations of a single device. For Greek Crosses (Fig. 8b) this is not the case.

From Fig. 9 it is observed that resistances extracted from van der Pauw structures (except for the 300 μm device) are significantly lower than those extracted from Greek Crosses. A slight increase of R_m is observed for larger devices. The reduced measured resistance may be related to the finite contact area (~2.5 × 0.1 μm^2) of the electrodes (i.e. not point-like contacts) in the van der Pauw structures [5, 15, 16].

Furthermore, a decrease is observed in R_m extracted from van der Pauw structures for smaller devices. This is most likely due to the fact that the edge of the ALD layer is situated further away from the electrodes for smaller devices,

thereby violating one of van der Pauw's boundary conditions that the contacts should be at the circumference of the sample [5]. This is supported by measurements on the 300 μm van der Pauw device in which the electrodes are close to the ALD TiN layer edge: they yield virtually the same values for R_m as extracted from Greek Crosses.

For Greek Cross devices, the sheet resistance ($R_{\square}$) can be calculated from R_m using a correction factor of $\pi/\ln(2)$[7]. The resistivity (ρ) is calculated from $R_{\square}$ and the layer thickness (averaged over all 5 devices). Values of 131 and 288 μΩcm are obtained for 7 and 4 nm ALD TiN, respectively. These results are shown in Fig. 10 together with results from literature [17]. The literature ρ-values are obtained from *in situ* SE modelling using Drude-Lorenz parameterization. The extraction of ρ includes correction for its temperature dependence: it is extracted at ~400 °C and calculated back to room temperature values using the temperature coefficient of resistance (TCR) (see section C). The same TCR value is used for all TiN layer thicknesses [18].

The error in our ρ-data originates from uncertainty in the ALD TiN layer thickness. The extracted resistivity values are slightly higher than the literature values, but still realistic [2, 17, 19]. This difference may be due to differences in material composition and/or the uncertainty in the layer thickness.

For van der Pauw devices it is more complicated to extract $R_{\square}$. As mentioned above, the contacts have finite size and are not always placed at the circumference of the ALD TiN layer structure, so a correction factor different from the standard correction factor of $\pi/\ln(2)$ has to be used. This factor can be derived in an analytical way [20], or from finite element (FE) modelling [21]. Using the analytical method, described in [20], correction factors for all vdP structures were calculated. These were confirmed by FE simulations [22]. Using these correction factors, ρ values of 130 and 290 μΩcm were found for 7 and 4 nm ALD TiN films, respectively. These values agree well with those obtained from GC structures.

B. Measurements at room temperature ('Design B')

For a 7 nm ALD TiN layer, *IV*-curves are measured from Greek Cross (GC) structures having *W* values of 8 and 50 μm. All devices are measured over all 4 orientations. The *IV*-curves of the first orientation are shown in Fig. 11. For both devices, linear *IV*-behaviour is observed. This is confirmed by plotting $d(V_m)/d(I_m)$, which is a constant function of I_m (see inset Fig. 11). By averaging $d(V_m)/d(I_m)$ values, R_m is calculated and averaged over the 4 orientations. R_m values of 45.2 Ω and 44.8 Ω are found for the 50 μm and 8 μm devices, of which ρ values of 143 and 142 μΩcm are extracted, respectively. These values are within 10% of the ρ value (131 μΩcm) found for GCs with 7 nm TiN of 'design A'. It is concluded the resistivities extracted from 'design A' are confirmed by the reference 'design B' for a 7 nm ALD TiN layer.

C. Measurements at elevated temperatures ('Design A')

Both van der Pauw and Greek Cross devices can be used for measurements at different temperatures to find the temperature coefficient of resistance (TCR) of the ALD TiN film. For a 7 nm ALD TiN film, resistance measurements in the range of 25 - 175 ºC are shown in Fig. 12. In Fig. 12a the measured resistance R_m of a 75 µm van der Pauw and a 75 µm Greek Cross device are shown. A linear fit through the data can be described as:

$$R_m = aT + R_0 \qquad (1)$$

where R_m is the V_m/I_m [Ω] and T is the temperature [ºC]. The temperature coefficient of resistance (β or TCR) [/ºC] can be extracted from the fit parameters a and R_0 by rewriting (1):

$$R_m = R_0(1+\beta T) \rightarrow \frac{R_m}{R_0} = \beta T + 1 \qquad (2)$$

where $\beta = a/R_0$ [23].

In Fig. 12b R_m/R_0 is plotted versus temperature for the same devices as in Fig. 12a. Although the absolute R_m values of the van der Pauw and the Greek Cross differ, it is observed that the normalized resistance values yield the same TCR (3.59×10^{-4} /ºC) for both types of devices. It is concluded, the same TCR value is extracted for vdP as for GC structures, without using the adapted correction factors.

The extracted TCR from Greek Cross devices of 3.5×10^{-4} /ºC is roughly 40% lower than the literature value of 5.5×10^{-4} /ºC, measured by Langereis and co-workers on an ALD TiN layer that is deposited under similar conditions[17, 18]. The difference is most likely due to a reduction of the TCR as a result of (the less temperature dependent) enhanced surface scattering which occurs for extremely thin films. Langereis and co-workers used a 33 nm thick film for the determination of their TCR, which is significantly thicker than our 7 nm film [17, 18].

D. Measurements at elevated temperatures ('Design B')

For a 7 nm ALD TiN film, resistance measurements for Greek Cross structures of 'design B', in the range of 25 - 175 ºC are shown in Fig. 13. Similar to the previous section, the TCR is extracted from these data, yielding values of 3.3×10^{-4} /ºC and 3.5×10^{-4} /ºC for the 50 µm and 8 µm device, respectively. These values agree well with the average TCR value (3.6×10^{-4} /ºC) found for both GCs and vdPs with 7 nm TiN of 'design A'. It is concluded that test structures of 'design A' and 'design B' yield the same TCR values for a 7 nm ALD TiN layer.

CONCLUSIONS

In this work, a novel test structure is presented for measuring the sheet resistance, based on buried electrodes on which the ultrathin film is deposited on a planar surface ('design A'). From electrical measurements on Greek Cross structures, resistivity values (ρ) are extracted of 288 and 133 μΩcm for 4 and 7 nm ALD TiN layers, respectively, which are independent of the device dimensions. These realistic values are extracted using the standard correction factor. For van der Pauw (vdP) devices, the same resistivity values can be extracted, using adapted correction factors obtained from either analytical or finite element methods. From Greek Cross structures, the temperature coefficient of resistance (TCR) of ALD TiN is extracted. For a 7 nm ALD TiN layer, a TCR value of 3.6×10^{-4} /ºC is found. For van der Pauw type structures, the same value is extracted, without using the adapted correction factors.

The second type of test structures contains Greek Cross structures only ('design B') and were fabricated to verify the results obtained from 'design A'. In this design, the ALD TiN thin film is deposited on a non-planar surface and follows the electrode topography. These test structures yield the same ρ- and TCR-values for a 7 nm ALD TiN layer as for 'design A'. We conclude that test structures of 'design A' can be used successfully for the extraction of both the resistivity and TCR of thin ALD TiN layers.

ACKNOWLEDGMENT

The authors thank M. Hoekman (LioniX B.V.) for help with CMP processing, T. Aarnink (MESA+) for help with the ALD of TiN, W. van den Einden (Philips) for help with the RTA and the Dutch Technology Foundation STW for financial support of this project (07682).

REFERENCES

[1] "International Technology Roadmap for Semiconductors: 2007 Update, International Sematech, 2007. Available from: http://public.itrs.net."
[2] M. Ritala and M. Leskelä, "Ch. 2: Atomic layer deposition," in *Handbook of thin film materials part 1: Deposition and processing of thin films*, vol. 1, H. S. Nalwa, Ed.: Academic Press, 2002, pp. 103-159.
[3] D. T. Castro, L. Goux, G. A. M. Hurkx, K. Attenborough, R. Delhougne, J. Lisoni, F. J. Jedema, M. A. A. t Zandt, R. A. M. Wolters, D. J. Gravesteijn, M. Verheijen, M. Kaiser, and R. G. R. Weemaes, "Evidence of the Thermo-Electric Thomson Effect and Influence on the Program Conditions and Cell Optimization in Phase-Change Memory Cells," in Proc. Elec. Dev. Meet., 2007, pp. 315-318.
[4] J. Sarkar and B. Gleixner, "Evolution of phase change memory characteristics with operating cycles: Electrical characterization and physical modeling," App. Phys. Let., vol. 91, pp. 233506-3, 2007.
[5] L. van der Pauw, "A Method of Measuring Specific Resistivity and Hall Effect of Discs of Arbitrary Shape," Phil. Res. Rep., vol. 13, pp. 1-9, 1958.
[6] L. van der Pauw, "A method of measuring the resistivity and Hall coefficient on lamellae of arbitrary shape," Phil. Tech. Rev., vol. 20, pp. 220-224, 1958.
[7] M. G. Buehler and W. R. Thurber, "An Experimental Study of Various Cross Sheet Resistor Test Structures," J. ECS., vol. 125, pp. 645-650, 1978.
[8] K. R. Williams, K. Gupta, and M. Wasilik, "Etch rates for micromachining processing - Part II," J. MEMS, vol. 12, pp. 761-778, 2003.
[9] S. Enderling, C. L. Brown, III, S. Smith, M. H. Dicks, J. T. M. Stevenson, M. Mitkova, M. N. Kozicki, and A. J. Walton, "Sheet resistance measurement of non-standard cleanroom materials using suspended Greek cross test structures," Trans. Sem. Man., vol. 19, pp. 2-9, 2006.

[10]L. Giraudet, S. Fauveaux, O. Simonetti, C. Petit, K. Blary, T. Maurel, and A. Belkhir, "Spin-coated conductive polymer film resistivity measurement using the TLM method," Synt. Mat., vol. 156, pp. 838-842, 2006.
[11]S. Enderling, M. H. Dicks, S. Smith, J. T. M. Stevenson, and A. J. Walton, "Thermal design considerations for Greek cross test structures," in Proc. ICMTS, 2003, pp. 8-13.
[12]S. Smith, "Sheet Resistance and Electrical Linewidth Test Structures for Semiconductor Process Characterisation," vol. PhD Thesis. Edinburgh, Scotland: University of Edinburgh, Scotland, 2003, pp. 224.
[13]Y. Sun, J. Shi, and Q. Meng, "Measurement of sheet resistance of cross microareas using a modified van der Pauw method," Sem. Sc. Tech., vol. 11, pp. 805-811, 1996.
[14]H. van Bui et.al., "Study of ALD TiN growth via in situ spectroscopic ellipsometry (SE)," J. ECS. (submitted), 2010.
[15]W. Versnel, "Analysis of symmetrical Van der Pauw structures with finite contacts," Sol.St. El., vol. 21, pp. 1261-1268, 1978.
[16]M. Cornils, M. Doelle, and O. Paul, "Sheet Resistance Determination Using Symmetric Structures With Contacts of Finite Size," Trans. El. Dev., vol. 54, pp. 2756-2761, 2007.
[17]E. Langereis, S. B. S. Heil, M. C. M. van de Sanden, and W. M. M. Kessels, "In situ spectroscopic ellipsometry study on the growth of ultrathin TiN films by plasma-assisted atomic layer deposition," J. Appl. Phys., vol. 100, pp. 023534, 2006.
[18]E. Langereis, "private communication," 2009.
[19]S. B. S. Heil, E. Langereis, F. Roozeboom, M. C. M. van de Sanden, and W. M. M. Kessels, "Low-temperature deposition of TiN by plasma-assisted atomic layer deposition," J. ECS, vol. 153, pp. G956-G965, 2006.
[20]D. S. Perloff, "Four-point sheet resistance correction factors for thin rectangular samples," Sol. St. El., vol. 20, pp. 681-687, 1977.
[21]N. M. P. Guillaume, M. W. Cresswell, R. A. Allen, S. Everist, and L. W. Linholm, "Comparison of sheet-resistance measurements obtained by standard and small-area four-point probing," in Proc. ICMTS, 1999, pp. 62-66.
[22]S. Smith and A. J. Walton, "private communication."
[23]R. C. Weast, *CRC Handbook of Chemistry and Physics*, 1st student ed: CRC Press, Inc., Boca Raton, Florida, USA, 1987.

FIGURES

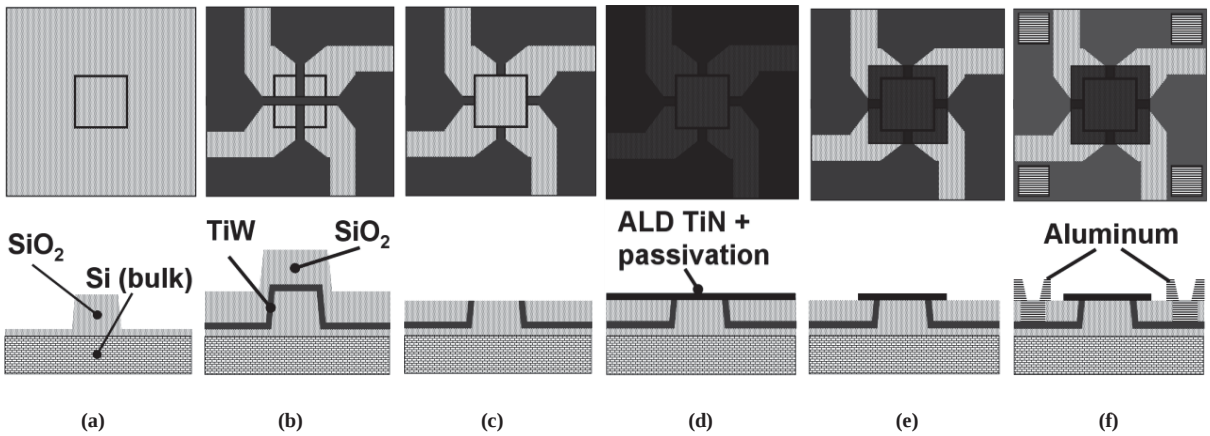

Fig. 1. 'Process archictecture A': fabrication scheme for a van der Pauw structure (top view (top) and cross-section (bottom)).

A [µm]	D [µm]	y [µm]
10	172	79
25	357	161
50	357	143
75	500	197
100	500	179
300	530	53

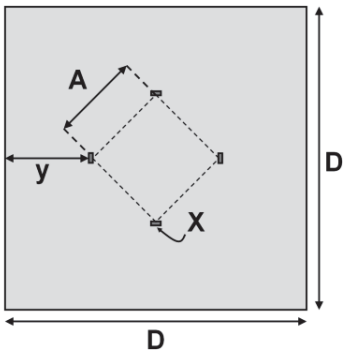

(a)

W [µm]
10
25
50
75
100

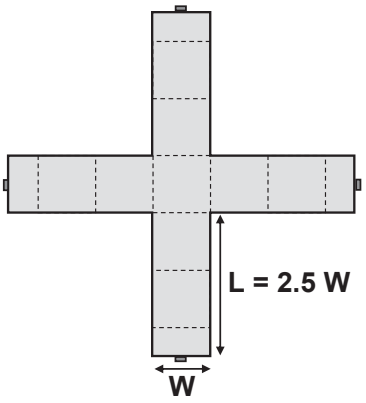

(b)

Fig. 2. Schematic design of a van der Pauw ('design A') (a) and Greek Cross (b) device ('design A & B'). The four contacts of the van der Pauw are situated at the corners of an imaginary square at a distance *A* that is centred with respect to the ALD film. The ALD film is patterned as a square with dimension *D*. *X* indicates the area of a single contact (2.5 µm × 0.1 µm for all devices). The Greek Cross is designed with the arm length *L* equal to 2.5 times the width *W*. This reduces the error in the extracted sheet resistance to < 1% while maintaining maximum sensitivity and minimal Joule heating in the arms of the cross [11-13]. Dashed lines indicate the (imaginary) squares.

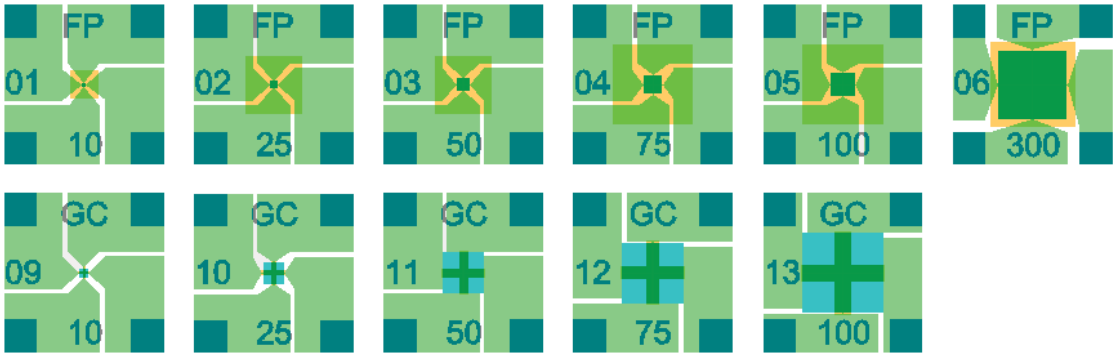

Fig. 3. Arrangement of vdP (names 'FP') and GC devices in a die of 'design A'. The size is 7 mm × 2.2 mm and is replicated 81 times over a 100 mm wafer.

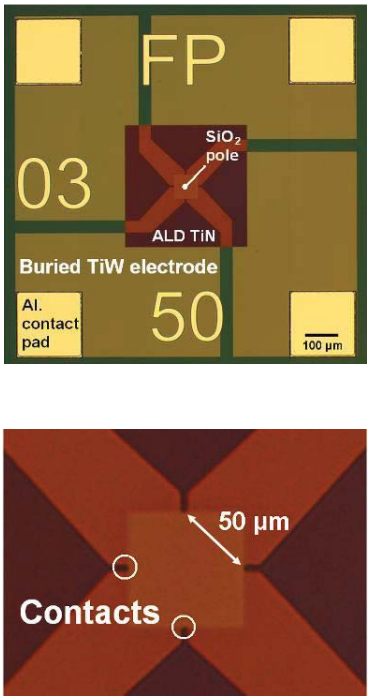

Fig. 4. Optical micrograph of a van der Pauw structure ('design A') with a probe-to-probe distance *A* of 50 µm. Whole structure (top) and close up of the electrodes (bottom).

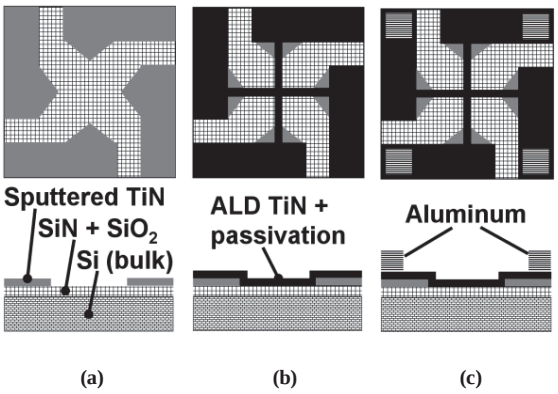

Fig. 5. 'Design B': fabrication scheme for a Greek Cross structure (top view (top) and cross-section (bottom)).

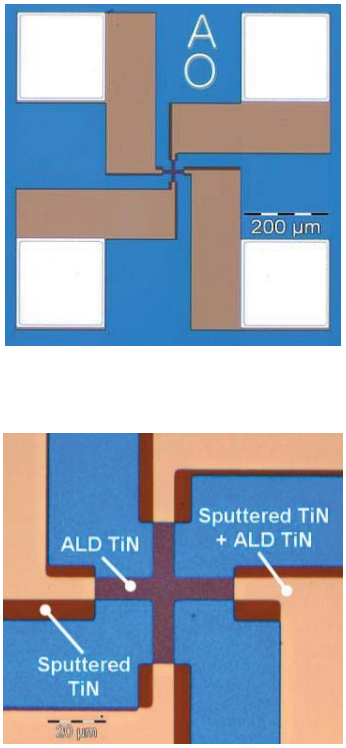

Fig. 6. Optical micrograph of an 8 µm Greek Cross structure (‘design B’). Whole structure (top) and close up of the centre (bottom).

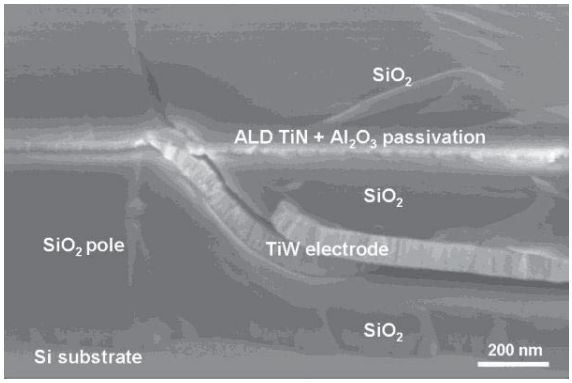

(a)

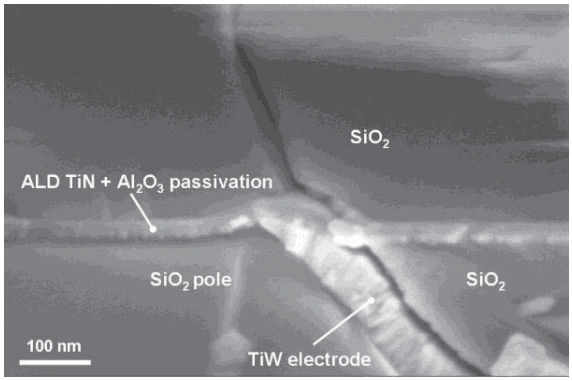

(b)

Fig. 7. Cross-section of the contact of the buried electrode and the ALD TiN layer ('design A'). Overview (a) and close-up (b).

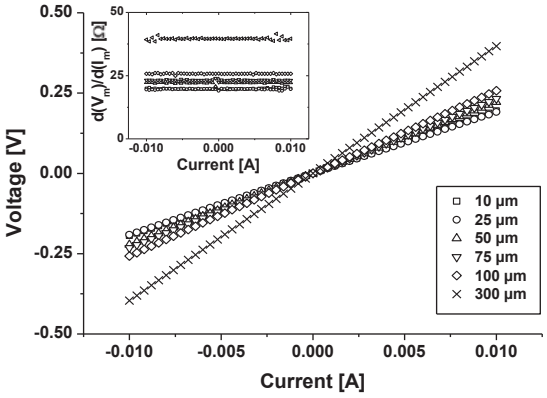

(a)

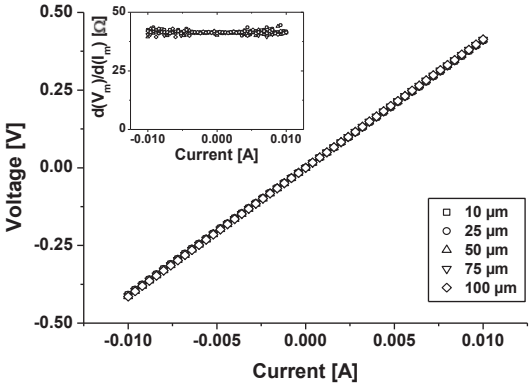

(b)

Fig. 8. Measured V_m versus I_m curves for van der Pauw (a) and Greek Cross (b) test structures ('design A') for 7 nm ALD TiN for one of the four measurement orientations. The inset shows the corresponding $d(V_m)/d(I_m)$ versus I_m plots. Dimensions in the legend refer to the probe-to-probe distance A (van der Pauw) and the W value of the Greek Cross. The extra noise in the inset in $d(V_m)/d(I_m)$ for large I_m-values is due to a change in the measurement range of the measurement apparatus during the measurement.

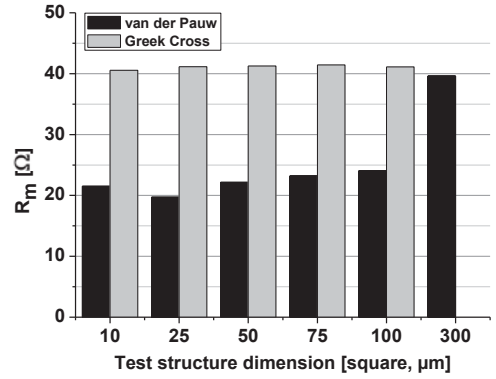

(a)

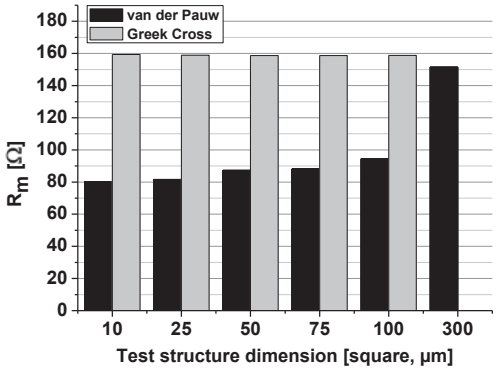

(b)

Fig. 9. Extracted resistances (V_m/I_m) from van der Pauw and Greek Cross structures ('design A') for 7 nm (a) and 4 nm (b) ALD TiN layers. Resistances are an average of the 4 measured orientations (see Fig. 4). Dimensions refer to the probe-to-probe distance *A* (van der Pauw) and the *W* value of the Greek Cross. For van der Pauw devices the probe-to-edge-distance (*y*) is different for each device (see fig. 2a).

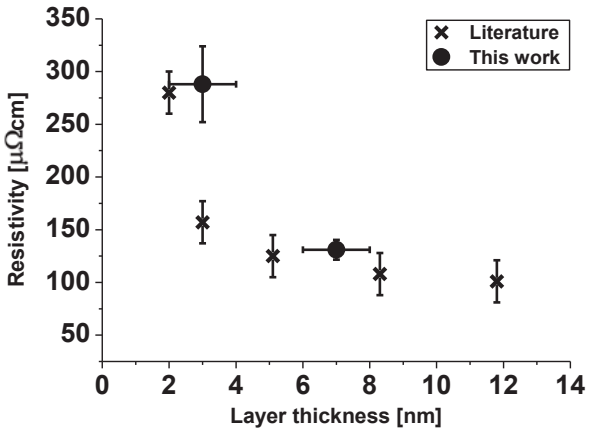

Fig. 10. Resistivity versus layer thickness for ALD TiN films ('design A'). Literature values are reprinted from [17]. The uncertainty in our data is due to uncertainties in the layer thickness, as derived from spectroscopic ellipsometer (SE) measurements.

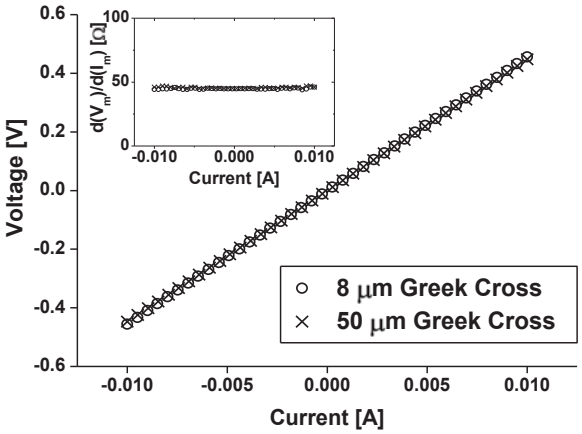

Fig. 11 Measured V_m versus I_m curves for Greek Cross structures ('design B') for 7 nm ALD TiN. The inset shows the corresponding dV_m/dI_m versus I_m. Dimensions refer to W value of the Greek Cross.

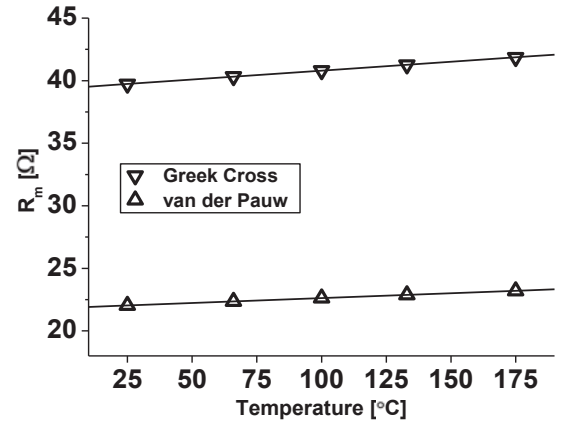

(a)

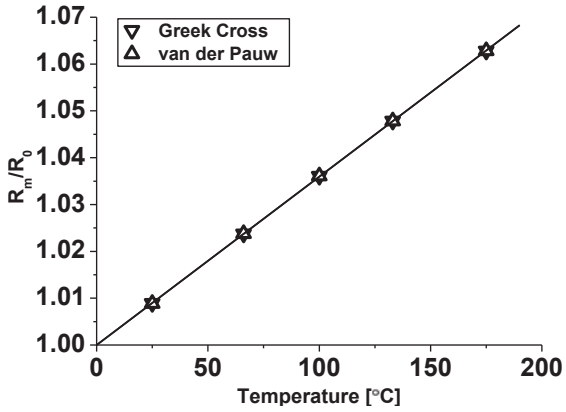

(b)

Fig. 12. Resistance versus temperature curves of 75 µm van der Pauw and 75 µm Greek Cross devices ('design A') for a 7 nm ALD TiN layer. (a) the measured resistance (R_m) and (b) R_m normalized on the (extrapolated) R_m value at 0 ºC (R_0). Lines are linear fits through the data. The temperature coefficient of resistance (TCR) is extracted from the slope of (b) (see text).

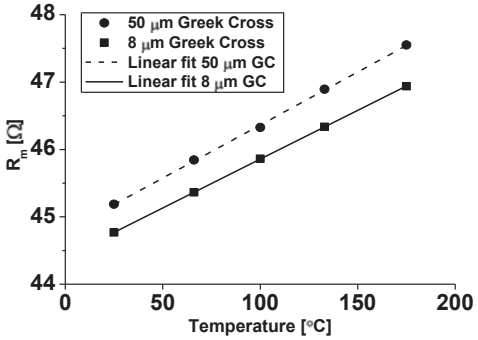

Fig. 13. Resistance versus temperature curves for Greek Cross devices ('design B') for a 7 nm ALD TiN layer. Lines are linear fits through the data. Dimensions refer to the *W* value of the Greek Cross.

CAPTIONS:

Fig. 1. 'Process archictecture A': fabrication scheme for a van der Pauw structure (top view (top) and cross-section (bottom)).

Fig. 2. Schematic design of a van der Pauw ('design A') (a) and Greek Cross (b) device ('design A & B'). The four contacts of the van der Pauw are situated at the corners of an imaginary square at a distance A that is centred with respect to the ALD film. The ALD film is patterned as a square with dimension D. X indicates the area of a single contact (2.5 µm × 0.1 µm for all devices). The Greek Cross is designed with the arm length L equal to 2.5 times the width W. This reduces the error in the extracted sheet resistance to < 1% while maintaining maximum sensitivity and minimal Joule heating in the arms of the cross [11-13]. Dashed lines indicate the (imaginary) squares.

Fig. 3. Arrangement of vdP (names 'FP') and GC devices in a die of 'design A'. The size is 7 mm × 2.2 mm and is replicated 81 times over a 100 mm wafer.

Fig. 4. Optical micrograph of a van der Pauw structure ('design A') with a probe-to-probe distance A of 50 µm. Whole structure (top) and close up of the electrodes (bottom).

Fig. 5. 'Design B': fabrication scheme for a Greek Cross structure (top view (top) and cross-section (bottom)).

Fig. 6. Optical micrograph of an 8 µm Greek Cross structure ('design B'). Whole structure (top) and close up of the centre (bottom).

Fig. 7. Cross-section of the contact of the buried electrode and the ALD TiN layer ('design A'). Overview (a) and close-up (b).

Fig. 8. Measured V_m versus I_m curves for van der Pauw (a) and Greek Cross (b) test structures ('design A') for 7 nm ALD TiN for one of the four measurement orientations. The inset shows the corresponding $d(V_m)/d(I_m)$ versus I_m plots. Dimensions in the legend refer to the probe-to-probe distance A (van der Pauw) and the W value of the Greek Cross. The extra noise in the inset in $d(V_m)/d(I_m)$ for large I_m-values is due to a change in the measurement range of the measurement apparatus during the measurement.

Fig. 9. Extracted resistances (V_m/I_m) from van der Pauw and Greek Cross structures ('design A') for 7 nm (a) and 4 nm (b) ALD TiN layers. Resistances are an average of the 4 measured orientations (see Fig. 4). Dimensions refer to the probe-to-probe distance A (van der Pauw) and the W value of the Greek Cross. For van der Pauw devices the probe-to-edge-distance (y) is different for each device (see fig. 2a).

Fig. 10. Resistivity versus layer thickness for ALD TiN films ('design A'). Literature values are reprinted from [17]. The uncertainty in our data is due to uncertainties in the layer thickness, as derived from spectroscopic ellipsometer (SE) measurements.

Fig. 11 Measured V_m versus I_m curves for Greek Cross structures ('design B') for 7 nm ALD TiN. The inset shows the corresponding dV_m/dI_m versus I_m. Dimensions refer to W value of the Greek Cross.

Fig. 12. Resistance versus temperature curves of 75 µm van der Pauw and 75 µm Greek Cross devices ('design A') for a 7 nm ALD TiN layer. (a) the measured resistance (R_m) and (b) R_m normalized on the (extrapolated) R_m value at 0 ºC (R_0). Lines are linear fits through the data. The temperature coefficient of resistance (TCR) is extracted from the slope of (b) (see text).

Fig. 13. Resistance versus temperature curves for Greek Cross devices ('design B') for a 7 nm ALD TiN layer. Lines are linear fits through the data. Dimensions refer to the *W* value of the Greek Cross.